

RESEARCH

Open Access



Enhanced therapeutic effects of hypoxia-preconditioned mesenchymal stromal cell-derived extracellular vesicles in renal ischemic injury

Fei Yuan^{1†}, Jie Liu^{2†}, Liang Zhong^{1†}, Pengtao Liu¹, Ting Li³, Kexin Yang³, Wei Gao³, Guangyuan Zhang^{4*}, Jie Sun^{1*} and Xiangyu Zou^{1,3*}

Abstract

Background Extracellular vesicles (EVs) secreted by mesenchymal stromal cells (MSCs) have been shown to provide significant protection against renal ischemia–reperfusion injury (IRI). Hypoxia has emerged as a promising strategy to enhance the tissue repair capabilities of MSCs. However, the specific effects of hypoxia on MSCs and MSC-EVs, as well as their therapeutic potential in renal IRI, remain unclear. In this study, we investigated the alterations occurring in MSCs and the production of MSC-EVs following hypoxia pre-treatment, and further explored the key intrinsic mechanisms underlying the therapeutic effects of hypoxic MSC-EVs in the treatment of renal IRI.

Methods Human umbilical cord MSCs were cultured under normoxic and hypoxic conditions. Proliferation and related pathways were measured, and RNA sequencing was used to detect changes in the transcriptional profile. MSC-EVs from both normoxic and hypoxic conditions were isolated and characterized. In vivo, the localization and therapeutic effects of MSC-EVs were assessed in a rat renal IRI model. Histological examinations were conducted to evaluate the structure, proliferation, and apoptosis of IRI kidney tissue respectively. Renal function was assessed by measuring serum creatinine and blood urea nitrogen levels. In vitro, the therapeutic potential of MSC-EVs were measured in renal tubular epithelial cells injured by antimycin A. Protein sequencing analysis of hypoxic MSC-EVs was performed, and the depletion of Glutathione S-Transferase Omega 1 (GSTO1) in hypoxic MSC-EVs was carried out to verify its key role in alleviating renal injury.

Results Hypoxia alters MSCs transcriptional profile, promotes their proliferation, and increases the production of EVs. Hypoxia-pretreated MSC-EVs demonstrated a superior ability to mitigate renal IRI, enhancing proliferation and reducing apoptosis of renal tubular epithelial cells both in vivo and in vitro. Protein profiling of the EVs revealed an accumulation of numerous anti-oxidative stress proteins, with GSTO1 being particularly prominent. Knockdown of GSTO1 significantly reduced the antioxidant and therapeutic effects on renal IRI of hypoxic MSC-EVs.

[†]Fei Yuan, Jie Liu, and Liang Zhong have contributed equally to this work.

*Correspondence:

Guangyuan Zhang

zgy0879@qq.com

Jie Sun

sunjie@scmc.com.cn

Xiangyu Zou

zouxiangyudy@126.com

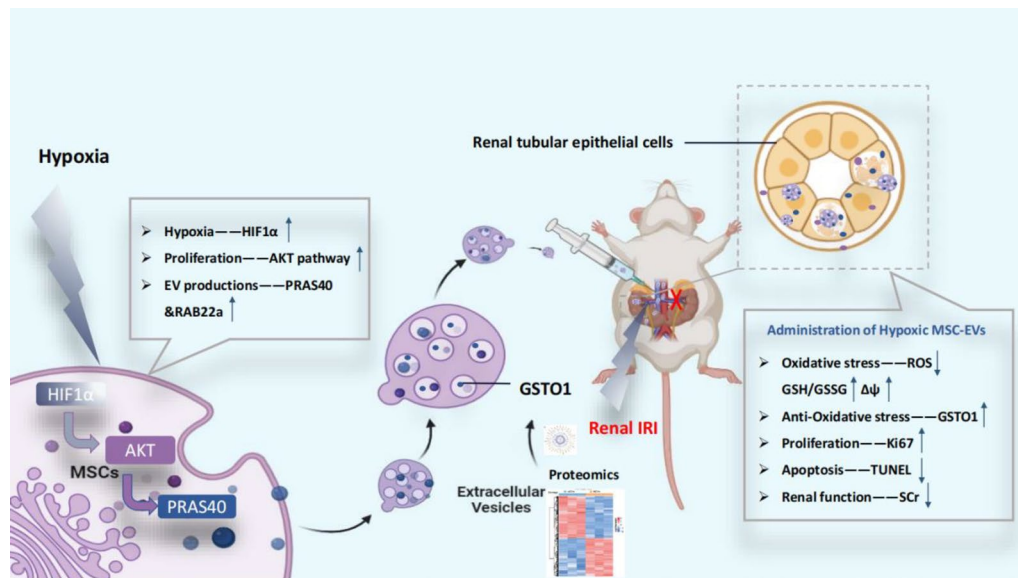
Full list of author information is available at the end of the article



Conclusions Hypoxia significantly promotes the generation of MSC-EVs and enhances their therapeutic effects on renal IRI. The antioxidant stress effect induced by GSTO1 is identified as one of the most critical underlying mechanisms. Our findings highlight that hypoxia-pretreated MSC-EVs represent a novel and promising therapeutic strategy for renal IRI.

Keywords Hypoxia pretreated, Mesenchymal stromal cells, Extracellular vesicles, Renal ischemia reperfusion injury, Anti-oxidative stress

Graphical Abstract



Background

Acute kidney injury (AKI), characterized by a rapid decline in renal excretory function, poses a serious threat to patient well-being and survival [1]. It is estimated that one in five adults and one in three children develop AKI during hospital stays, often as a result of sudden kidney failure or damage [2]. Renal ischemia–reperfusion injury (IRI) is a leading cause of AKI, commonly occurs in patients undergoing sepsis or surgical procedures such as kidney transplantation [3]. Currently, therapeutic options for AKI remain limited. While pharmacological interventions like angiotensin-converting enzyme inhibitors and angiotensin receptor blockers have been employed to modulate renal function [4], they have proven ineffective in reversing the progression of kidney dysfunction. Consequently, there is an urgent need for more effective strategies to alleviate kidney tissue damage and promote regeneration are urgently needed.

Mesenchymal stromal cells (MSCs) possess remarkable self-renewal capabilities and have demonstrated efficacy in treating a wide range of conditions, including tissue

damage repair, inflammation suppression, and immune modulation [5]. MSCs have shown significant potential in promoting kidney repair following AKI by alleviating tubulointerstitial damage [6–8]. Furthermore, extracellular vesicles (EVs) secreted by MSCs act as crucial cellular regulators in numerous biological processes [9–11]. Characterized by a lipid bilayer structure, MSC-EVs facilitate intercellular communication by delivering a diverse array of cargos, including RNAs, proteins, and lipids [12, 13]. Notably, MSC-EVs have been reported to mitigate renal damage caused by IRI and to support cellular repair mechanisms [14]. Compared to MSCs, EVs exhibit lower immunogenicity and enhanced biological safety, making them promising candidates for therapeutic applications in various diseases.

Hypoxia pre-treatment significantly enhances protective capabilities of MSCs for injured tissues and organs. Hypoxia-pretreated MSCs have demonstrated the ability to alleviate spinal cord injury and promote bone repair. Additionally, hypoxic conditions influence the production and composition of MSC-EVs. However, the precise

effects of hypoxic preconditioning on MSC-EV production, as well as the underlying mechanisms by which hypoxic EVs facilitate tissue repair, remain poorly understood. Therefore, in this study, we aim to investigate the impact of hypoxia on human umbilical cord MSCs and validate the therapeutic efficacy of hypoxic EVs in a rat model of IRI-induced AKI. Furthermore, we seek to elucidate the potential mechanisms underlying the therapeutic effects of hypoxic EVs through proteomic analysis.

Materials and methods

Cell culture

MSCs were prepared and identified as described in our previous study [15]. In brief, umbilical cord tissues were cut and attached individually to culture plates. The collection and subsequent use of the umbilical cord were approved by the Institutional Ethical Review Committee of Shanghai Children's Medical Center, School of Medicine, Shanghai Jiao Tong University. Cells were cultured with a medium composed of α -MEM (12571063, Gibco) containing 5% UltraGRO™-Advanced cell culture supplement (HPCFDCGL50, Helios) and incubated in a 5% CO₂ environment at 37 °C. When the cell confluency reached 90%, MSCs were passaged at a 1:5 ratio, and the medium was replaced every 2 days.

The rat renal tubular epithelial cell line NRK-52E (CL-0174, Procell Life Science & Technology Co., Ltd.) was cultured in DMEM (11965092, Gibco) supplemented with 5% fetal bovine serum (A5669701, Gibco). Cells were incubated in an incubator with 5% CO₂ at 37 °C. When cells reached 70% confluency, they were passaged at a 1:3 ratio. The medium was changed every 2 days.

Hypoxia pre-treatment of MSCs

MSCs were plated in 10 cm dishes and cultured until reached approximately 80%–90% confluence for downstream experiments. Hypoxia pre-treatment is conducted by different concentration of oxygen (a humidified atmosphere containing 5% CO₂ with 10%, 5% or 3% O₂ at 37 °C) for 24 h. In subsequent experiments, a 5% O₂ concentration was used for treatment. In the normoxic group, cells were incubated in an incubator with 5% CO₂ and 21% O₂ at 37 °C.

CCK-8 assay

The cell proliferation of MSCs and NRK-52E were determined by CCK-8 assay (K1018, APEX BIO) following the instructions. The absorbance at 450 nm wavelength was measured by a microplate reader (Thermo Fisher).

Transcriptomic analysis

Total RNA was extracted using Fast Pure Cell/Tissue Total RNA Isolation Kit (RC101, Vazyme) according to

the manufacturer's instructions. The primary experimental procedures for transcriptome sequencing analysis include RNA quantification and qualification, library preparation for transcriptome sequencing, clustering, and sequencing, and data analysis. HTSeq v0.6.0 was used to quantify the number of reads mapped to each gene. The FPKM of each gene was calculated based on its length and the number of mapped reads. Differential expression analysis of the two groups was performed using the DESeq2 R package (1.10.1), with an adjusted *p*-value < 0.05 was considered indicative of significant differential expression. GO (Gene Ontology) enrichment analysis of differentially expressed genes (DEGs) was carried out using the clusterProfiler R package. DEGs were correlated with annotations, including GO terms. Significantly enriched GO terms were identified based on corrected *p*-values less than 0.05. The transcriptome sequencing analysis in this study was supported by BGI-gene Co, Ltd.

Isolation and purification of MSC-EVs

The extraction of EVs was performed as described in the previously published literature [15]. MSCs incubated under normoxic (21% O₂) and hypoxic (5% O₂) conditions were cultured in UltraGRO™-Advanced cell culture supplement-free media for 24 h, and the supernatants were subsequently collected for MSC-EVs extraction. In brief, the supernatants were centrifuged at 2,000 g for 20 min at 4 °C to remove cell debris, followed by a second centrifugation at 100,000 g (Beckman Coulter, Fullerton, CA) for 1 h at 4 °C. The pellet was re-suspended in cold PBS for washing and centrifuged again under the same conditions to collect the EVs. The isolated EVs were stored at – 80 °C.

Characterization of EVs

The morphology of EVs was observed using transmission electron microscopy (TEM). The particle size was measured via nanoparticle tracking analysis (NTA). Surface markers including CD9, D63, and CD81 were analyzed by Western blot analysis. Protein concentration of EVs derived from 1×10^7 MSCs was quantified using the bicinchoninic acid (BCA) assay kit (A55860, Thermo Fisher).

Western blot analysis

Western blot was performed as previously described [16]. The following primary antibodies were used: anti-CD9 (dilution 1:1000; ab236630, Abcam), CD63 (dilution 1:1000; ab134045, Abcam), CD81 (dilution 1:1000; ab79559, Abcam), hypoxia-inducible factor-1 α (HIF-1 α) (dilution 1:1000; 14,179, CST), serine/threonine kinase (AKT) (dilution 1:1000; 9272, CST), phosphorylated

Serine/threonine kinase (p-AKT) (dilution 1:1000; 9271, CST), phosphorylated proline-rich AKT substrate of 40 kDa (p-PRAS40) (dilution 1:1000; ab151719, Abcam), RAB22a (dilution 1:1000; ab137093, Abcam), Glutathione S-Transferase Omega 1 (GSTO1) (dilution 1:1000; 15,124-1-AP, Proteintech), Beta Actin (β -actin) (dilution 1:1000; ab8226, Abcam).

Labeling and location of MSC-EVs in vivo and in vitro

To label MSC-EVs, MSCs were incubated with 10 μ M PKH-26 dye (HY-D1451, MCE) in serum-free culture medium at room temperature for 15 min, followed by two washes with sterile PBS to remove excess dye. The cultures were continued for MSCs 2 days and observed using fluorescence microscopy (Stellris 8, Leica). The supernatants were used to isolate PKH-26-labeled EVs in the same procedure as above. In this way, the free dye could be removed to the utmost extent. For in vivo studies, PKH-26-labeled EVs were administered into rats via the inferior vena cava. After 48 h, the kidneys of model rats underwent tissue fixation, dehydration, embedding and sectioning for subsequent observation of EVs' location under a fluorescent microscope. Renal tissues showed green auto-fluorescence. In vitro, PKH-26-labeled EVs were added to the medium of NRK-52E cells cultured on coated coverslips for 24 h. Cells were fixed and stained for further analysis. After coverslips coated for cell culture were fixed with 4% paraformaldehyde, cytoplasm and nucleus were localized with Phalloidin (A12379, Thermo Fisher) and DAPI (62,248, Thermo Fisher), respectively. The intracellular location of EVs was then observed under a fluorescence microscope.

Rats and surgical preparation

The ethics Committee of Shanghai Children's Medical Center, School of Medicine, Shanghai Jiao Tong University approved this study. Eight-week-old male Sprague-Dawley rats (180–200 g), purchased from Shanghai Jihui Experimental Animal Breeding Co., Ltd., were used in this study. All experimental rats were housed in an environment with controlled temperature and humidity and provided a normal diet. An AKI model was established as previously described [17]. Rats were anesthetized with 2% isoflurane administered via the respiratory tract. In brief, rats were subjected to random allocation into four groups ($n=6$), comprising those undergoing sham surgery (sham), IRI treated with PBS (IRI), IRI treated with normoxic MSC-EVs (IRI/nEVs), or IRI treated with hypoxic MSC-EVs (IRI/hEVs). A mid-abdominal incision was employed for the excision of the right kidney and temporary occlusion of the left renal pedicle for a duration of 45 min, after which the hemostatic clamp was released to restore blood flow to the kidney. Then 1 ml

EVs at a protein concentration of 100 μ g/ml quantified by BCA kit was administered immediately to the respective groups via the inferior vena cava. Sham-treated subjects underwent an identical surgical intervention, albeit devoid of occlusion of the renal pedicle. Rats were euthanized by excessive carbon dioxide under anesthesia conditions at 48 h after EVs injection. The kidney tissue and serum samples were collected for the following examinations. Rats were housed in the same animal facility and underwent relevant procedures performed by the same surgical personnel. All animal experiments were reported in line with the ARRIVE guidelines 2.0.

Histological examination and renal function assessment

Renal histological examination and renal function assessment were performed as previously described [17]. Parts of the left kidney were fixed in 4% paraformaldehyde, then dehydrated in ethanol and embedded in paraffin. Kidney tissue blocks were cut into 4 μ m sections and subjected to hematoxylin–eosin (H&E) staining. Subsequently, the stained sections were viewed using light microscopy. A score was given based on the grade of tubular necrosis, brush border loss, cast formation and tubular dilatation in ten randomly chosen areas. The histological scoring was determined in a blind manner based on the following criteria refer to previous literature: (0) none; (1) 0–10%; (2) 11–25%; (3) 26–45%; (4) 46–75% and (5) 76–100% [17].

Renal cell apoptosis was assessed by using TUNEL staining (C1091, Beyotime). Renal tissue was analyzed using TUNEL immunohistochemistry, while coverslips coated for cell culture were analyzed using TUNEL immunofluorescence. Both renal tissues and coverslips coated for cell culture underwent fixation, permeabilization with 0.1% Triton X-100 (A110694, Sangon Biotech) for 10 min followed by wash with PBS. TUNEL staining was performed following manufacturer's guidelines. The numbers of TUNEL-positive tubular cells in renal tissue were quantified by counting the cells in 10 randomly chosen non-overlapping fields per slide. The average fluorescence intensity in cultured cells was quantified by image J (Version 1.54 h 15, Wisconsin, USA) in 10 randomly chosen non-overlapping fields per slide.

Renal cell proliferation was assessed using immunohistochemical staining for Ki67. The kidney tissue paraffin sections were permeabilized with 0.3% Triton X-100, followed by blocking with 10% donkey serum and incubation with the primary antibodies against Ki67 (dilution 1:200; ab16667, Abcam). Subsequently, the sections were incubated with secondary anti-rabbit IgG conjugated to horseradish peroxidase (HRP) (dilution 1:200; 7074S, CST). Positive staining was detected via a 3,3'-diaminobenzidine (D8001, Sigma-Aldrich) reaction. Tissue

images were captured using a microscope (DMI4000 B, Leica).

The blood urea nitrogen (BUN) and serum creatinine (SCr) levels were determined by the Urea Nitrogen Assay Kit (D799849, Sangon Biotech) and Creatinine Assay kit (D799853, Sangon Biotech) according to the manufacturers' protocols. Blood samples from rats were collected 48 h after EV injection. The blood was centrifuged at 2500 rpm for 10 min, and the supernatant was collected and stored at -80°C for further analysis.

Proteomic analysis of MSC-EVs

Normoxic and hypoxic EV samples were prepared and analyzed in triplicate ($n=3$). The primary experimental procedures for proteomics analysis include protein extraction, trypsin digestion, liquid chromatograph mass spectrometer (LC-MS/MS) analysis and data analysis. The resulting MS/MS data were processed using the DIA-NN search engine (Version 1.8). Tandem mass spectra were searched against the Human UniProt database (20,376 entries) concatenated with a reverse decoy database. Subcellular localization of the differentially expressed proteins in MSC-EVs was analyzed using PSORTb software (v3.0). The Kyoto Encyclopedia of Genes and Genomes (KEGG) database was employed for KEGG pathway enrichment analysis. Reactome pathway annotation and WikiPathways pathway annotations were identified by Reactome database and WikiPathways database. The proteomic analysis in this study was supported by Jingjie PTM BioLabs.

Assessment the levels of reactive oxygen species (ROS) in vivo and in vitro

The fluorescent probe Dihydroethidium (DHE) (S0063, Beyotime) was used to detect the ROS levels of fresh-frozen kidney tissue. On the other hand, 10 mM 2',7'-dichlorodihydro fluorescein diacetate (DCFH-DA, S0033S, Beyotime) was used to assess the ROS production of NRK-52E in situ visualization. Nuclei were stained with DAPI before captured the image under microscopy. Fluorescence intensity of staining was measured by Image J. Six representative visual fields of each group were counted.

Assessment the levels of mitochondrial membrane potential ($\Delta\psi\text{m}$)

NRK-52E were plated in confocal petri dishes. Cells were treated with 100 μM Antimycin (AMA) and then loaded with the potentiometric dye 500 nM TMRE (C2001S, Beyotime) at 37°C in cell culture chamber for 20 min and Hoechst 33,342 (C1027, Beyotime) for 5 min. The staining was viewed by a confocal scanning microscope after washing 3 times with PBS.

Assessment of GSH and GSSG levels

The concentration of GSH and GSSG of both NRK-52E and fresh rat kidney tissue were quantified by the GSH content detection kit (colorimetric method) (D799613, Sangon Biotech) and the GSSG content detection kit (colorimetric method) (D799615, Sangon Biotech). For tissue, weigh 0.1 g of fresh kidney tissue, and then add 1 mL of Reagent One. Use a homogenizer gently grind tissue samples on ice. Centrifuge samples at 8000 g and 4°C for 10 min and save the supernatant for testing. Then, proceed with the tests as the manufacturer's instructions. The absorbance at 412-nm wavelength was measured by a microplate reader (Aligent).

Cell transfection of siRNA

MSCs were seeded in a 10-cm dish at 70% confluence one day prior to transfection. Nucleotides formed transfection complexes with Lipofectamine 2000 (11,668,027, Thermo Fisher), and were added to cells and incubated for 6–8 h prior to refreshing the medium. Small interfering RNAs (siRNAs) were synthesized by Sangon Biotech Co., Ltd. based on the following sequences. siGSTO1-214: sense 5'-GCCUGAGUGGUUCUUUAA GAATT-3', antisense 5'-UUCUUAAAGAACCACUCA GGCTT-3'. hGSTO1-411: sense 5'-CCUUGGUAGGAA GCUUUUUUATT-3', antisense 5'-UAAUAAAGCUUC CUACCAAGGTT-3'. hGSTO1-411: sense 5'-GUUAAA UGAGUGUGUAGACCATT-3', antisense 5'-UGGUCU ACACACUUUAACTT-3'. FAM labeled siRNA was used to evaluate transfection efficiency. Cells exhibiting stable green fluorescence were considered successfully transfected.

(See figure on next page.)

Fig. 1 Hypoxia promotes MSCs proliferation and alters their transcriptomes. **A:** Morphology of MSCs under normoxic and hypoxic conditions observed via light microscope (scale bar = 200 μm). **B:** CCK-8 assays comparing cell viability between normoxic ($n=3$) and hypoxic groups ($n=3$) ($*P < 0.05$). **C:** Western blot analysis showing HIF-1 α , AKT, p-AKT, and β -actin expression levels in hypoxic ($n=4$) and normoxic ($n=4$) conditions. **D:** Statistical analysis of Western blot results, showing protein expression levels of HIF-1 α , AKT, and p-AKT ($*P < 0.05$). **E:** Heatmap clustering analysis of DEGs in hypoxic ($n=3$) and normoxic ($n=3$) conditions. **F:** GO enrichment analysis of the DEGs

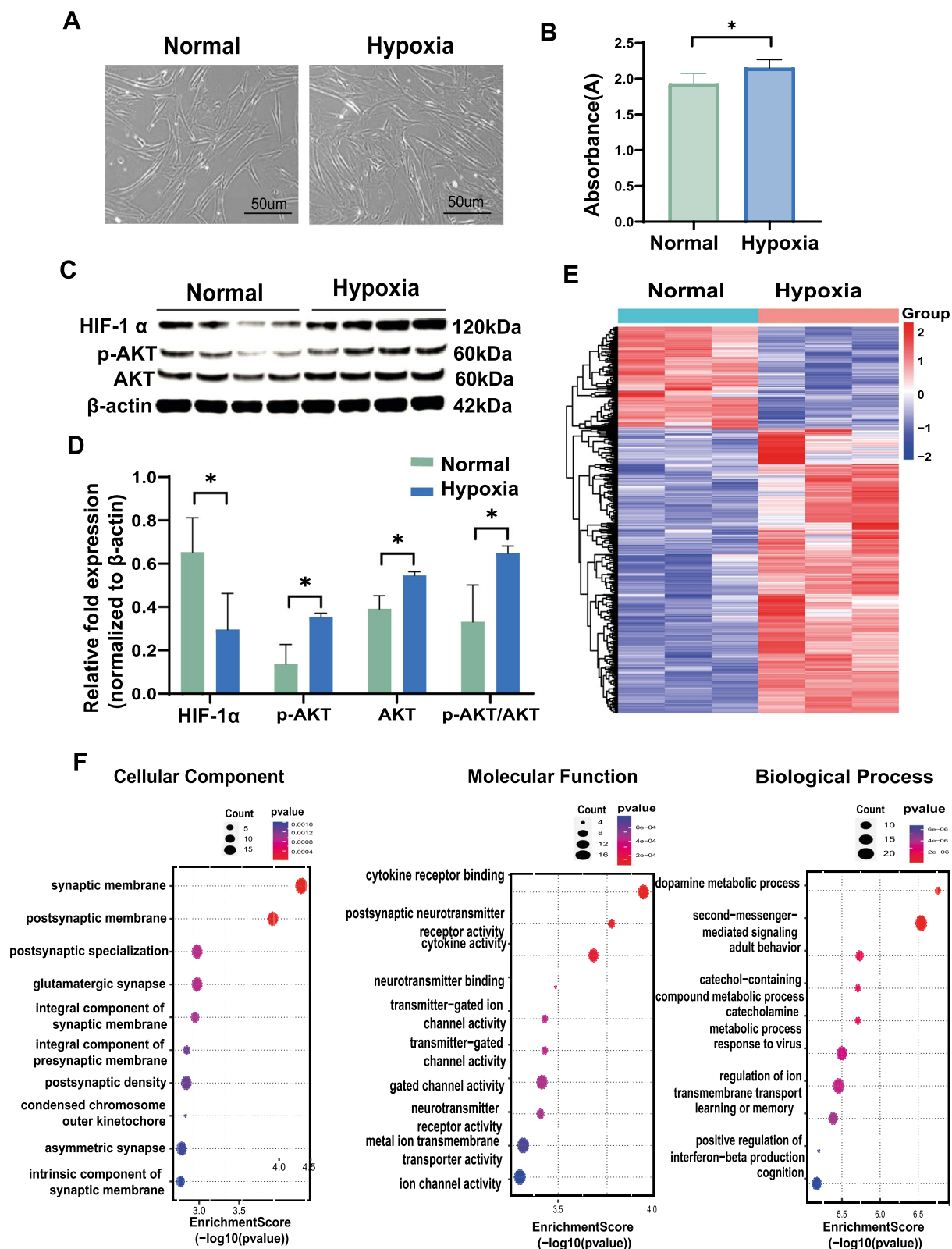


Fig. 1 (See legend on previous page.)

Quantitative real-time PCR (qPCR)

Total RNA was initially extracted from both treated and control cell samples using a TRIzol™ Reagent (15,596,026, Thermal Fisher), following the manufacturer's protocol. Subsequently, RNA samples were reverse transcribed into complementary DNA (cDNA) using a HiScript IV RT SuperMix for qPCR (+gDNA wiper) kit (R423-01, Vazyme). Specific primers designed against the sequences of interest and a reference gene were utilized for qPCR amplification. The qPCR reactions were carried out in triplicate using a ChamQ Universal SYBR qPCR Master Mix (Q711-02, Vazyme) to monitor DNA synthesis in real time. Fluorescence data collected during the annealing phase were used to calculate the threshold cycle values for each target gene. Expression levels were normalized to β -actin. Here is the sequence of primers: β -actin sense 5'-CACCATTGGCAATGAGCGGTTC-3' and antisense 5'-AGGTCTTTGCGGATGTCCACGT-3'; GSTO1 sense 5'-GAAGACGACCTTCTTTGGTGGC-3' and antisense 5'-CTTCATGGCTGCCATCCACAGT-3'.

Statistical analysis

Statistical analysis was conducted using GraphPad Prism 10.0. We used the Shapiro–Wilk test to assess the normality of the data distribution. Data that were normally distributed are presented as mean \pm standard deviation (SD). For comparing two groups, an unpaired t-test was used to determine statistical significance. For multiple group comparisons, one-way analysis of variance (ANOVA) was performed. $P < 0.05$ was deemed statistically significant.

Results

Hypoxia promotes proliferation and alters transcriptome of MSCs

After 24 h of hypoxia pre-treatment, MSCs retained their characteristic spindle-shaped morphology with a radial distribution but exhibited a significantly increased degree of cell fusion compared to those in normoxic conditions (Fig. 1A). The CCK-8 assay confirmed a marked increase in cell viability in the hypoxic group, indicating that hypoxia substantially promotes cell proliferation

(Fig. 1B). Western blot analysis further demonstrated a significant upregulation of HIF-1 α expression in MSCs under hypoxic conditions. Additionally, activation of the AKT signaling pathway, known to be associated with cell proliferation, was observed, with significant increases in the levels of AKT, phosphorylated AKT (p-AKT), and the p-AKT/AKT ratio in the hypoxic group (Fig. 1C,D).

Transcriptomic analysis of hypoxia-pretreated MSCs revealed profound alterations in gene expression profiles, as illustrated by the heatmap of DEGs (Fig. 1E). GO analysis showed a significant enrichment of these DEGs in cellular membrane components and transporter activities, both of which are closely associated with the production and secretion of EVs (Fig. 1F).

Alterations in the MSC characteristics and yield of EVs following hypoxia preconditioning

TEM revealed that EVs derived from both normoxic and hypoxic conditions displayed similar morphologies, appearing as round or elliptical vesicles with intact structures (Fig. 2A). The expression levels of specific membrane protein markers associated with EVs, including CD9, CD63, and CD81 were assessed by Western blot. The results demonstrated increased expression of CD9 and CD63 in hypoxic EVs, while the alteration in CD81 expression was not statistically significant (Fig. 2B,C).

Measurement of protein concentration in EVs produced by 1×10^7 MSCs revealed that the EVs from hypoxia pre-treated MSCs had a significantly higher concentration compared to those from the normoxic group (Fig. 2D). NTA demonstrated that the size of EVs ranged from 50 to 500 nm in both groups, indicating no significant difference (Fig. 2E,F). However, the particle concentration in the hypoxic group was significantly elevated compared to the normoxic group (Fig. 2G).

Furthermore, we examined the expression of proteins involved in EV secretion in MSCs, specifically PRAS40 and RAB22a. PRAS40 expression exhibited a marked increase under 5% oxygen conditions, accompanied by a significantly elevated expression of HIF-1 α under both 10% and 5% oxygen conditions. Although RAB22a expression did not increase under 10% oxygen

(See figure on next page.)

Fig. 2 Changes in EVs production and characterization following hypoxia pre-treatment. **A:** TEM images showing EV morphology under normoxic and hypoxic conditions (scale bar = 200 nm). **B:** Western blot analysis of EV markers, including CD9, CD63, and CD81 in hypoxic (n = 3) and normoxic (n = 3) conditions. **C:** Relative quantification and statistical analysis of CD9, CD63, and CD81 expression levels (* $P < 0.05$). **D:** Quantification of EV protein concentration derived from 1×10^7 MSCs under normoxic (n = 5) and hypoxic (n = 5) conditions (* $P < 0.05$). **E:** NTA analysis showing size distribution and diameter of EVs. **F:** Statistical analysis of EV diameter in hypoxic (n = 5) and normoxic (n = 5) conditions. **G:** Statistical analysis of EV particle concentration in hypoxic (n = 5) and normoxic (n = 5) conditions (**** $P < 0.0001$). **H:** Western blot analysis of HIF-1 α , PRAS40, RAB22a, and β -actin levels at 21% (normoxic, n = 3), 10% (n = 3), 5% (n = 3), and 3% O₂ conditions (n = 3). **I:** Statistical analysis of HIF-1 α protein expression levels normalized to β -actin (* $P < 0.05$). **J:** Western blot analysis of PRAS40 protein levels normalized to β -actin (* $P < 0.05$). **K:** Western blot analysis of RAB22a protein levels normalized to β -actin (* $P < 0.05$).

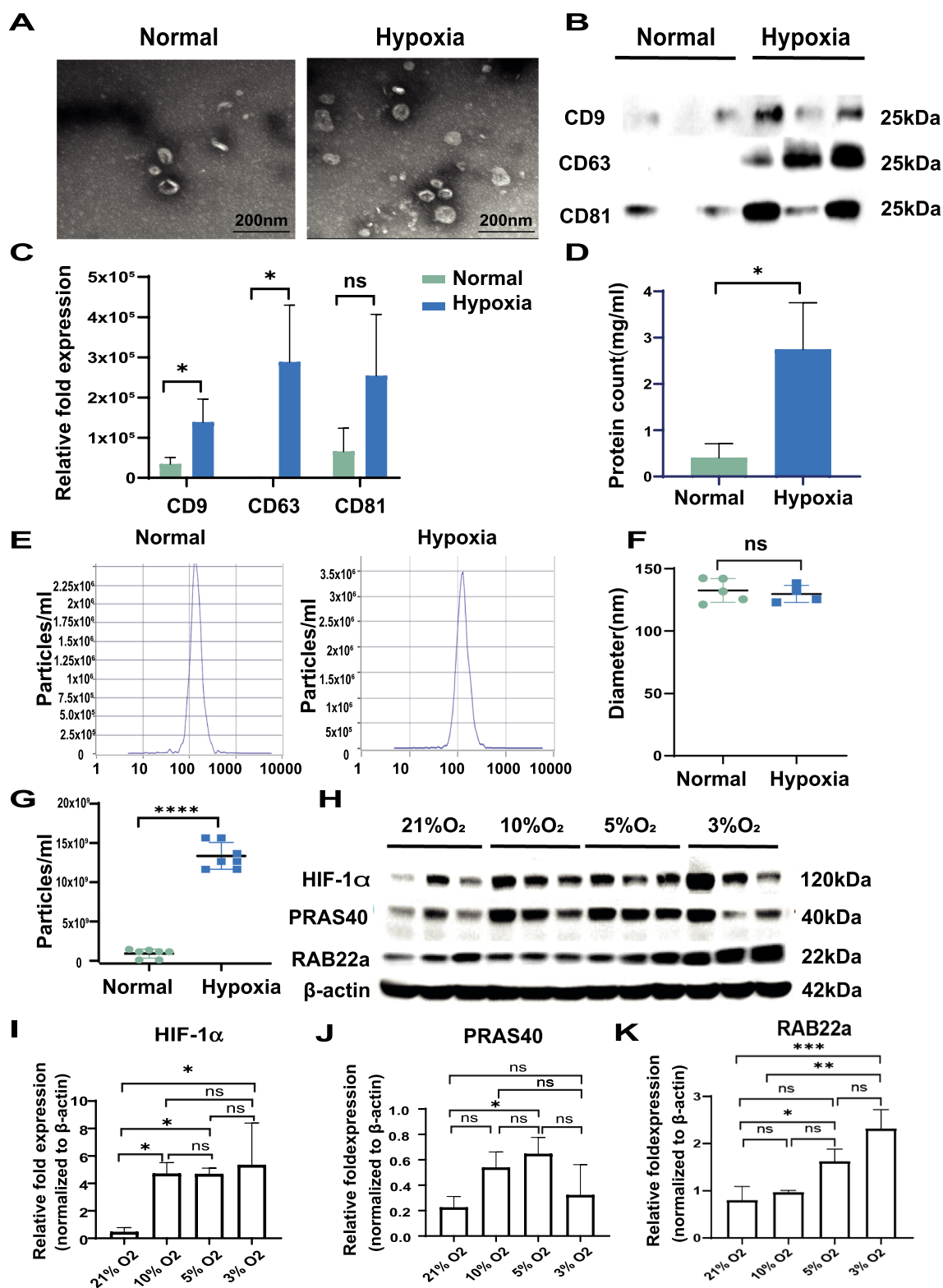


Fig. 2 (See legend on previous page.)

conditions, but it was significantly up-regulated under 5% and 3% oxygen conditions (Fig. 2H–K).

Hypoxic EVs exhibited superior efficacy in promoting recovery from renal IRI

PKH26-labeled EVs were systemically administered to rats undergoing IRI. After 48 h, PKH26 fluorescence was clearly detectable within the kidney tissue (Fig. 3A). H&E staining revealed numerous necrotic areas in the proximal epithelium and abundant tubular protein casts in the IRI-affected kidneys. In contrast, treatment with both normoxic and hypoxic EVs resulted in a reduction of tubular lesions (Fig. 3B). Renal injury scoring, based on structural alterations, demonstrated that hypoxic EVs were significantly more effective at alleviating morphological changes associated with IRI compared to their normoxic counterparts (Fig. 3E). Ki67 staining, a marker of cell proliferation, showed enhanced tissue proliferation following IRI, which was further augmented by hypoxic EV treatments (Figs. 3C,F). TUNEL staining revealed IRI-induced apoptosis, which was markedly attenuated by the administration of both normoxic and hypoxic EVs, with hypoxic EVs exhibiting greater efficacy (Fig. 3D,G).

Renal function was assessed by measuring SCr and BUN. Rats with renal IRI treated with PBS exhibited a rapid increase in SCr and BUN levels. In contrast, treatment with normoxic and hypoxic EVs significantly attenuated these increases (Fig. 3H,I). Notably, hypoxic EV-treated kidneys showed lower renal injury scores, higher Ki67 expression, fewer apoptotic cells, and reduced SCr levels compared to those treated with normoxic EVs.

MSC-EVs promote anti-apoptosis of renal tubular epithelial cells in vitro

To model hypoxic injury to renal tubular epithelial cells, rat tubular epithelial cell line NRK-52E were exposed to AMA, an inhibitor of mitochondrial electron transport chain. As shown in Fig. 4A, AMA induced a dose-dependent reduction in NRK-52E cell viability, with a concentration of 100 μ M causing approximately a 50% decrease in cell viability. Treatment with both normoxic EVs and hypoxic EVs restored cell viability (Fig. 4B).

To investigate the uptake of MSC-EVs by renal tubular epithelial cells in vitro, MSCs were labeled with PKH-26, enabling the secreted EVs to carry red fluorescence (Fig. 4C). Internalization of PKH26-labeled EVs was confirmed in NRK-52E cells. Quantitative analysis demonstrated that hypoxic EVs exhibited significantly enhanced cellular uptake compared to normoxic EVs (Fig. 4D,F).

TUNEL staining demonstrated that AMA induced significant apoptosis in renal tubular epithelial cells. Both normoxic EVs and hypoxic EVs effectively attenuated cell apoptosis, with hypoxic EVs showing superior efficacy in protecting renal tubular epithelial cells from AMA-induced injury (Fig. 4E,G).

Hypoxia preconditioning up-regulated antioxidant stress pathway revealed by the proteomics of EVs

To elucidate the underlying mechanism by which hypoxic EVs exhibit superior efficacy for renal IRI, we conducted mass spectrometry analysis of the proteomic cargo of EVs. PCA clearly distinguished the proteomic signatures of hypoxic EVs from those of normoxic EVs, highlighting hypoxia-induced alterations in the protein profiles of MSC-EVs (Fig. 5A). We identified significant differences in protein expression levels between the two groups, with 264 proteins up-regulated and 288 proteins down-regulated in hypoxic EVs ($P < 0.05$) (Fig. 5B). Among these significant regulated proteins, GSTO1, an enzyme involved in the redox reaction of GSH, exhibited the most pronounced difference (Fig. 5C). Unsupervised hierarchical clustering analysis further validated the distinct protein patterns between normoxic and hypoxic EVs, as shown in the heatmap (Fig. 5D). Subcellular localization classification of the differentially expressed proteins indicated that the predominant proteins were extracellular (38.59%) and cytoplasmic (19.75%) (Fig. 5E). Functional enrichment analysis of up-regulated proteins demonstrated significant enrichment in GSH metabolism-related pathways, such as cysteine and methionine metabolism and glutathione metabolism, as identified by KEGG analysis (Fig. 5F). Additionally, there was notable enrichment of pathways associated with nuclear factor erythroid 2-related factor 2 (NRF2), a critical regulator of cellular oxidative stress resistance. This includes pathways related to

(See figure on next page.)

Fig. 3 Hypoxia EVs attenuate renal IRI in rat **A:** Localization of MSC-EVs labeled with PKH-26 in IRI kidneys, with DAPI staining for nuclei; background shows spontaneous green fluorescence of the kidney (scale bar = 100 μ m). **B:** H&E staining of rat kidneys across different groups (scale bar = 100 μ m): sham surgery (Sham), renal IRI injected with PBS (IRI), with normoxic EVs (IRI/nEVs), or with hypoxic EVs (IRI/hEVs). **C:** Representative images of Ki67-positive cells in the tubulointerstitial area (scale bar = 100 μ m). **D:** Representative images of apoptotic cells identified by TUNEL staining (scale bar = 100 μ m). **E:** Statistical analysis of kidney injury scores assessed from histological slides (n = 6). **F:** Quantification of Ki67-positive cells per high-power field (HPF) (n = 6). **G:** Quantification of apoptotic cells per HPF (n = 6). **H:** SCr levels across different groups (μ mol/L) (n = 6). **I:** BUN levels in different groups (μ g/mL) (n = 6). (* $P < 0.05$, ** $P < 0.01$, *** $P < 0.001$, **** $P < 0.0001$)

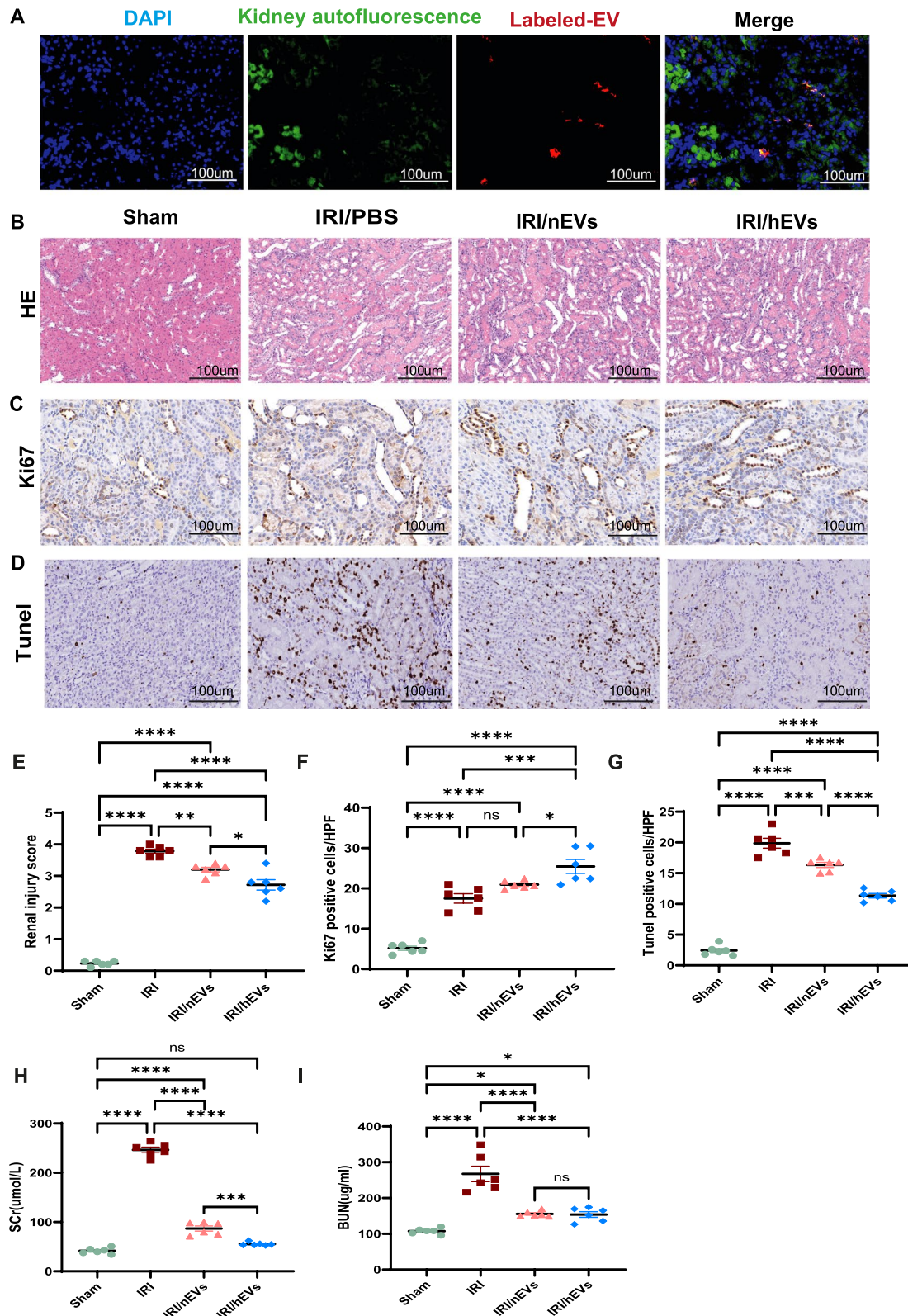


Fig. 3 (See legend on previous page.)

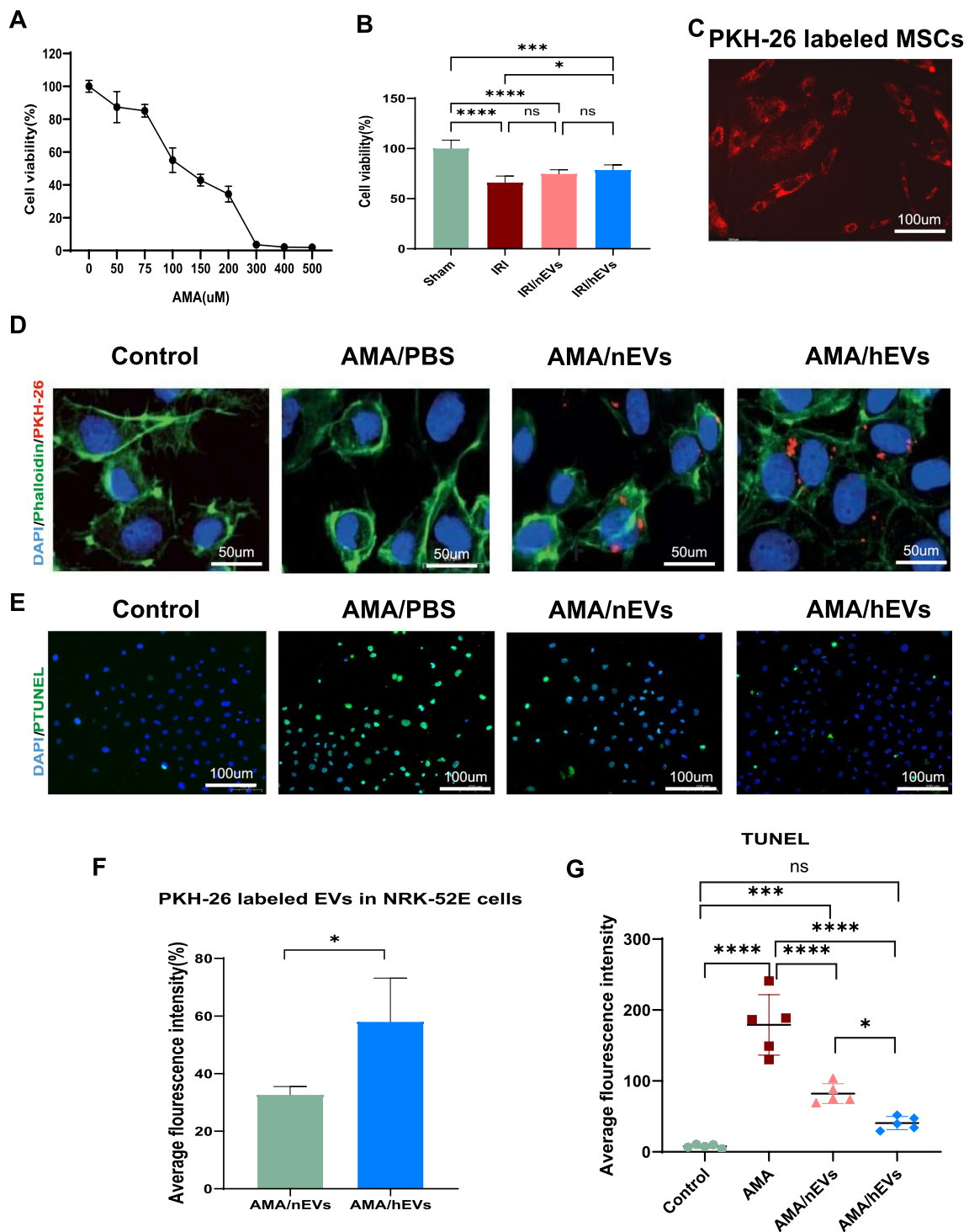


Fig. 4 Effects of hypoxic EVs on NRK-52E cells under AMA-induced injury. **A:** CCK-8 assay demonstrating the toxicity of various concentrations of AMA on NRK-52E cells (n=5). **B:** Cell viability of NRK-52E exposed to 100 μM AMA for 24 h across different treatment groups (n=5). **C:** MSCs labeled with PKH-26 (scale bar = 100 μm). **D:** Internalization of PKH-26 labeled EVs in the cytoplasm of NRK-52E (scale bar = 50 μm; blue: DAPI-stained nuclei, green: Phalloidin-stained cytoskeleton, red: PKH-26). **E:** Representative images of TUNEL staining in NRK-52E (scale bar = 200 μm). **F:** Quantification of internalized PKH-26-labeled EVs derived from normoxic (n=3) and hypoxic MSCs (n=3) in NRK-52E (*P < 0.05). **G:** Quantification of apoptotic cells HPF (n=5) (*P < 0.05, **P < 0.01, ***P < 0.001, ****P < 0.0001)

nuclear events mediated by NFE2L2, the KEAP1-NFE2L2 pathway, photodynamic therapy-induced NRF2 survival signaling, and the NRF2 pathway itself (Fig. 5G,H). Together, these findings suggest that hypoxia preconditioning enhances the expression of antioxidant stress-related proteins in MSC-EVs.

Validation of hypoxic EVs in alleviating renal IRI via antioxidant mechanisms

We first evaluated the differential effects of hypoxic and normoxic EVs on oxidative stress in rat kidney tissue. The results demonstrated that IRI significantly elevated ROS levels. Notably, hypoxic EVs markedly reduced ROS levels in IRI-affected kidneys compared to normoxic EVs (Fig. 6A,C). In vitro assays with NRK-52E cells exposed to AMA corroborated this trend, showing that ROS production and mitochondrial membrane potential changes mirrored those observed in rat kidney tissue (Fig. 6B,D,E). GSH plays a pivotal role in antioxidant defense and maintaining intracellular redox balance. In NRK52E cells, we assessed the intracellular levels of GSH, GSSG, and the GSH/GSSG ratio following EV treatment. LC-MS analysis revealed that AMA significantly reduced GSH levels while increasing GSSG levels, thereby decreasing the GSH/GSSG ratio. However, hypoxic EVs significantly restored GSH and GSSG levels, surpassing the restorative effects of normoxic EVs. Ultimately, the GSH/GSSG ratio in hypoxic EV group saw a significant increase, even reaching levels comparable to the sham group (Fig. 6F–H). Proteomic analysis revealed significant alterations in enzymes associated with GSH metabolism, including glutathione S-transferases (GSTs), glutathione synthetase (GSS), glutathione reductase (GSR), and glutathione peroxidase 1 (GPx) (Fig. S1A–F). GSTs, GSS, and GSR showed increased levels in hypoxia-preconditioned EVs, while GPx1 levels were reduced. Within the GSH metabolism pathway, GSS contributes to GSH synthesis, GSR converts GSSG back into GSH, and GSTs facilitate the conjugation of GSH with oxidative metabolic byproducts. In contrast, GPx drives the conversion of GSH to GSSG (Fig. S1G). Furthermore, a significant accumulation of superoxide dismutase (SOD) was observed in hypoxic EVs (Fig. S1H–I).

Next, the levels of TGF β , interleukins, growth factors, and chemokines in hypoxia-preconditioned EVs were

quantified. The results revealed that hypoxic EVs led to the upregulation of several soluble mediators, including TGF β 1, PDGFRA, VEGFC, and CCL2 (Fig. S2A–F). Additionally, renal protein levels of IL-10 and VEGFA were measured following EV treatment. However, the changes in IL-10 and VEGFA levels in the kidneys were not statistically significant (Fig. S2G–I).

We further validated the protein level of GSTO1, identified as the most differentially expressed protein in hypoxic EVs. The results confirmed that GSTO1 was upregulated in both hypoxia pre-treated MSCs and derived EVs (Figs. 6I–K). To investigate the role of GSTO1 in mitigating oxidative stress in hypoxic EVs, we knocked down GSTO1 using three different siRNAs. Except for siGSTO1-214, both siGSTO1-411 and siGSTO1-601 effectively silenced the mRNA and protein expression of GSTO1 in MSCs (Fig. 6L,M). Hypoxic EVs from MSCs transfected with both siGSTO1-411 and siGSTO1-601 didn't reduce the ROS levels of renal tubular epithelial cells as effectively as those transfected with a negative control siRNA (Fig. 6N,O). Furthermore, GSTO1 knockdown diminished the ability of the hypoxic EVs to restore the mitochondrial membrane potential in the renal tubular epithelium (Fig. S3A,C) and reduced the protective effect against AMA-induced apoptosis (Fig. S3B,D).

Upon treating IRI model rats with hypoxic EVs in which GSTO1 was knocked down, we observed notable changes. ROS level significantly increased compared to the control group receiving hypoxic EVs (Fig. S4A,D). Additionally, there was a noticeable decrease in Ki67 expression and an increase in apoptosis (Fig. S4B–C,E–F). Further analysis of kidney function revealed that hypoxic EVs with GSTO1 knockdown were less effective in mitigating elevated SCr and BUN levels resulting from IRI compared to the hypoxic EVs group (Fig. S5A,B). Taken together, these findings indicate that GSTO1 in hypoxic EVs is essential for alleviating renal IRI.

Discussion

IRI is a leading cause of AKI, resulting in damage to renal tubules and rapid deterioration of renal function. The current study demonstrates that hypoxia not only stimulates the proliferation of MSCs but also enhances the secretion of EVs. Additionally, MSC-EVs pre-treated with

(See figure on next page.)

Fig. 5 Hypoxia up-regulated antioxidant proteins in MSC-EVs. **A:** PCA distinguishing normoxic (n = 3) and hypoxic EVs (n = 3). **B:** Summary of protein types in EVs, with red indicating up-regulated and blue indicating down-regulated proteins. **C:** Top 30 proteins showing the most significant differences in expression. **D:** Heatmap clustering analysis of differentially expressed proteins. **E:** Subcellular localization analysis of up-regulated and down-regulated proteins. **F:** KEGG functional enrichment analysis of up-regulated differential proteins. **G:** WikiPathways enrichment analysis of up-regulated differential proteins. **H:** Reactome pathway enrichment analysis of up-regulated differential proteins

hypoxia exhibit a pronounced ability to protect against renal IRI. Importantly, we have presented novel evidence that hypoxia pre-treated MSC-EVs mitigate acute renal IRI through an anti-oxidative stress mechanism, with the antioxidant protein GSTO1 playing a crucial role in this protective process.

Conventional in vitro cell culture typically occurs under ambient oxygen conditions (21% O₂), referred to as 'normoxia'. In contrast, in vivo, MSCs are often located in niches with lower oxygen levels [18]. Culturing MSCs under hypoxic conditions aims to mimic this natural microenvironment. MSCs residing in hypoxic niches, with oxygen tensions ranging from 3 to 9%, retain their capacity for self-renewal, proliferation, migration, and differentiation [19, 20]. While previous studies have demonstrated that hypoxia preconditioning can enhance MSC proliferation and differentiation [21], the precise mechanisms remained unclear. In our study, we revealed that hypoxia activates the HIF-1 α /AKT signaling pathway to promote MSC proliferation. The cellular response to hypoxic stress is primarily mediated by HIF-1 α [22], and overexpression of HIF-1 α has been shown to enhance MSC proliferation and osteogenic differentiation [23]. The AKT signaling pathway plays a critical role in cell proliferation, and previous research has indicated that HIF-1 α contributes to the upregulation of p-AKT protein expression [24, 25]. These findings collectively support the involvement of the HIF-1 α /AKT pathway in MSC proliferation under hypoxic conditions.

MSCs contribute to tissue repair through endocrine or paracrine mechanisms, with EVs being one of their main means of communication [26]. These EVs play a crucial role in tissue repair by delivering proteins and genetic materials. Importantly, EV production is influenced by the surrounding microenvironment. The impact of MSC-EVs can be amplified under certain physical and biological stimuli, such as hypoxia, lipopolysaccharide, and TNF- α . These conditions not only boost EV production but may also modify their contents, ultimately enhancing their beneficial effects [27–30]. The RAB

family comprises key signaling molecules involved in EVs production, while PRAS40 is involved in the release of EVs following cellular stress [31, 32]. The production of MSC-EVs significantly increased under hypoxic culture conditions, with the activation of RAB22a and PRAS40 observed in MSCs in this study. Furthermore, the plasma membrane plays a crucial role in shaping and facilitating the functions of EVs during their generation. It is actively involved in cell signaling, membrane adaptability, and uptake by recipient cells. Interestingly, our transcriptomic analysis of MSCs revealed that hypoxia activates signaling pathways related to cell membrane components and transporter activities, both of which are associated with enhanced EV production.

Several studies have documented that hypoxic EVs are effective in mitigating organ ischemia injury, such as in the brain and limbs, by transporting microRNAs or proteins [33–35]. Zhang et al. [36] reported that hypoxic preconditioning of MSCs can enhance the repair of injured kidneys, with increased angiogenesis and antioxidant effects playing a role. Building on this, the therapeutic effects of hypoxic EVs on renal ischemia–reperfusion injury (IRI) were explored in this study. The results indicated that hypoxia preconditioning enhances the ability of MSC-EVs to repair IRI kidneys, improving both renal morphology and function. During AKI, tubular cell apoptosis and proliferation occur. Both in vivo and in vitro experiments demonstrated that hypoxia preconditioning of MSC-EVs significantly reduced tubular cell apoptosis and promoted their proliferation, demonstrating a stronger protective effect against injury.

To further investigate the underlying mechanisms, our results revealed that hypoxic preconditioning enhances the production of MSC-derived EVs, leading to a significant increase in EV particle number and protein concentrations. This increase may partly explain the enhanced therapeutic efficacy observed with hypoxic EVs. Additionally, EVs exert their effects through biologically active internal components, including proteins, lipids, and nucleic acids. However, the primary contributor among

(See figure on next page.)

Fig. 6 Hypoxic EVs alleviate acute renal IRI through the cargo of antioxidant proteins. **A:** Representative images of reactive oxygen species (ROS) fluorescence in rat kidneys (scale bars = 100 μ m). **B:** Representative images of mitochondrial membrane potential injury in NRK-52E cells (scale bars = 50 μ m). **C:** Quantitative analysis of ROS fluorescence intensity in rat kidneys (n = 5). **D:** ROS fluorescence quantified in NRK-52E following 24-h exposure to 100 μ M AMA (n = 5). **E:** Quantitative analysis of mitochondrial membrane potential fluorescence intensity in NRK-52E cells (n = 5). **F:** GSH levels across different experimental groups (n = 5). **G:** GSSG levels across different experimental groups (n = 5). **H:** GSH/GSSG ratio across different experimental groups (n = 5). **I:** Western blot analysis of GSTO1 expression levels in MSCs and EVs following hypoxic treatment. **J:** Statistical analysis of GSTO1 protein expression in MSCs, normalized to β -actin, as determined by Western blot (n = 3). **K:** Statistical analysis of GSTO1 protein expression in EVs, normalized by total protein concentration and volume (n = 3). **L:** mRNA expression levels of GSTO1 post-transfection with GSTO1-targeting siRNA, assessed by qPCR (n = 3). **M:** Protein expression levels of GSTO1 post-transfection with GSTO1-targeting siRNA, evaluated by Western blot (n = 2). **N:** Representative images of ROS fluorescence in NRK-52E (scale bars = 50 μ m). **O:** Quantitative analysis of ROS fluorescence in NRK-52E (n = 5) (* P < 0.05, ** P < 0.01, *** P < 0.001, **** P < 0.0001)

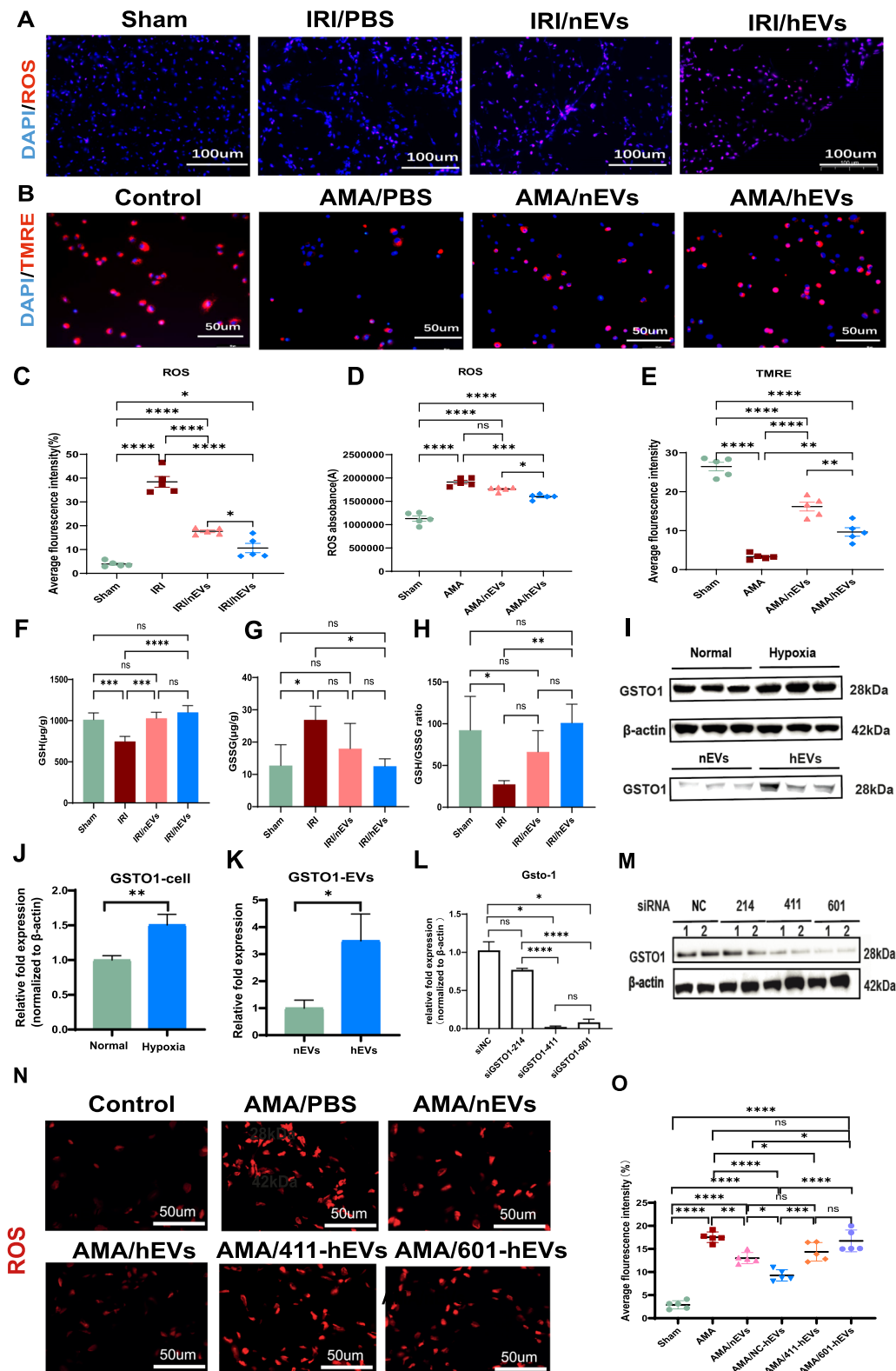


Fig. 6 (See legend on previous page.)

these components remains unclear. While substantial research has focused on the alterations of miRNAs within EVs, less attention has been paid to their protein content, which can directly influence recipient cells [37]. Recently, EVs have emerged as a novel mechanism for protein delivery [38]. Eirin et al. [39] emphasized in their study on MSC-EV-mediated kidney injury repair that the delivery of IL-10 protein is a key factor in the protective effects of MSC-EVs. In this study, the protein levels in hypoxia preconditioned EVs were examined through proteomic analysis. Various injury repair-related factors were found to be altered, including proteins associated with oxidative stress.

Oxidative stress plays a crucial role in the pathogenesis of ischemic kidney injury, and it has been established that MSC-EVs can reduce oxidative reactions and protect kidney function [40, 41]. In this study, MSC-EVs were also found to significantly reduce oxidative stress levels in injured kidneys, with hypoxic EVs exhibiting an even greater effect, highlighting their potent antioxidant properties. We observed a significant accumulation of oxidative stress-related proteins in hypoxic EVs, particularly enzymes involved in GSH metabolism and superoxide dismutase. Among all differentially expressed proteins, GSTO1 was one of the most notably upregulated proteins, which is an important enzyme that promotes the reduction of ROS through redox reactions involving GSH. GSTO1 has been shown to play a significant role in protecting the function of kidneys in end-stage renal disease [42]. It has also been reported that GSTO1 is involved in regulating oxidative stress and exerting protective effects in various diseases [43]. To further investigate the role of GSTO1 in hypoxic EVs, GSTO1-knockdown hypoxic EVs were obtained and used to treat ischemic renal injury. The data showed that, in the absence of GSTO1, the antioxidant effects of hypoxic EVs were significantly diminished, along with a reduction in their protective effects on tubular cells, ultimately leading to impaired kidney function protection. This finding suggests that the antioxidant protein GSTO1 plays a pivotal role in the protective effects of hypoxic EVs against renal IRI.

Conclusions

This study demonstrates that EVs derived from hypoxia-preconditioned MSCs provide renal protection against IRI. The antioxidant protein cargo, particularly GSTO1, plays a pivotal role in mitigating acute renal IRI. These findings highlight a promising therapeutic avenue for the clinical treatment of renal IRI.

Abbreviations

ACEIs	Angiotensin-converting enzyme inhibitors
AKI	Acute kidney injury

AKT	Serine/threonine kinase
AMA	Antimycin A
ARBs	Angiotensin receptor blockers
BUN	Blood urea nitrogen
CCL2	C–C motif chemokine ligand 2
DEGs	Differential express genes
ETC	Mitochondrial electron transport chain
EVs	Extracellular vesicles
GO	Gene ontology
GSTO1	Glutathione S-transferase omega 1
GSS	Glutathione synthetase
GSR	Glutathione reductase
GPx	Glutathione peroxidase
H&E	Hematoxylin–eosin
HIF-1 α	Hypoxia-inducible factor-1 α
huMSCs	Human umbilical cord MSCs
IL-10	Interleukin-10
IRI	Ischemia–reperfusion injury
KEGG	Kyoto encyclopedia of genes and genomes
MSCs	Mesenchymal stromal cells
NRF2	Nuclear factor erythroid 2–related factor 2
NTA	Nanoparticle tracking analysis
p-AKT	Phosphorylated serine/threonine kinase
PBS	Phosphate-buffered saline
PCA	Principal component analysis
PDGFRA	Platelet-derived growth factor receptor α
p-PRAS40	Phosphorylated proline-rich AKT substrate of 40 kDa
RAB22a	RAB22a, Member RAS oncogene family
ROS	Reactive oxygen species
SCr	Serum creatinine
SOD	Superoxide dismutase
TEM	Transmission electron microscopy
TGF β	Transforming growth factor β
VEGFC	Vascular endothelial growth factor C

Supplementary Information

The online version contains supplementary material available at <https://doi.org/10.1186/s13287-025-04166-z>.

Additional file 1.

Acknowledgements

The authors declare that they have not used AI-generated work in this manuscript.

Author contributions

FY, JL, LZ and PT L: experiments conducting, data acquirement and original manuscript preparation; FY, JL, LZ, PT L and XY Z: manuscript editing/validation and data analysis; WG, TL, KXY and XY Z: technical support and experimental assistance; GY Z, JS and XY Z: study design guidance, manuscript reviewing and editing; JS and XY Z: project supervision and funding acquisition. All authors read and approved the final manuscript.

Funding

This work was supported by grants from the National Natural Science Foundation of China (Grant No. 81900618); the Tai-Shan Scholar Program from Shandong Province, China (Grant No. tsqn202103116); the Pudong New Area Science and Technology Development Fund (Grant No. PKJ2020-Y04); the Natural Science Foundation of Fujian Province (Grant No. 2023J01183); the Program of Scientific and Technological Development of Weifang (Grant No. 2023GX026).

Availability of data and materials

All datasets to support current study are available from the corresponding author on reasonable request. The sequence data in the current study will be available in NCBI's BioProject and can be accessed by the public (ID: PRJNA1064232). The mass spectrometry proteomics data have been deposited

to the ProteomeXchange Consortium via the PRIDE partner repository with the dataset identifier PXD057088.

Declarations

Ethical approval and consent to participate

The project has been approved by the ethics committee of Shanghai Children's Medical Center, Shanghai Jiao Tong University School of Medicine. All human subjects gave informed consent for tissue donation. Project title: "The study on the mechanism by which hypoxia promotes mesenchymal stem cell-derived extracellular vesicle production and enhances the repair capacity of ischemia–reperfusion kidney injury", protocol number SCMCIRB-Y2019005, approved 2019/2/25. For animal experiments, the study was approved by the Shanghai Children's Medical Center, Shanghai Jiao Tong University School of Medicine, project title: "The study on the mechanism by which hypoxia promotes mesenchymal stem cell-derived extracellular vesicle production and enhances the repair capacity of ischemia–reperfusion kidney injury", protocol number SCMCACUC-K2019042, approved 2019/2/15.

Consent for publication

All authors agree to submission of the manuscript and agree to publication.

Competing interests

The authors declare that they have no competing interests.

Author details

¹Department of Urology, Shanghai Children's Medical Center, Shanghai Jiao Tong University School of Medicine, Shanghai 200127, China. ²Department of Neurology, Shanghai Children's Medical Center, Shanghai Jiao Tong University School of Medicine, Shanghai, China. ³School of Basic Medical Sciences, Shandong Second Medical University, Weifang, China. ⁴Department of Urology, Zhongda Hospital, Southeast University, Nanjing 210009, Jiangsu Province, China.

Received: 16 October 2024 Accepted: 21 January 2025

Published online: 04 February 2025

References

- Kellum JA, Romagnani P, Ashuntantang G, Ronco C, Zarbock A, Anders HJ. Acute kidney injury. *Nat Rev Dis Primers*. 2021;7:52.
- Aghajani Nargesi A, Lerman LO, Eirin A. Mesenchymal stem cell-derived extracellular vesicles for kidney repair: current status and looming challenges. *Stem Cell Res Ther*. 2017;8:273.
- Bonventre JV, Yang L. Cellular pathophysiology of ischemic acute kidney injury. *J Clin Invest*. 2011;121:4210–21.
- Guan C, Li C, Xu L, Che L, Wang Y, Yang C, et al. Hospitalized patients received furosemide undergoing acute kidney injury: the risk and prediction tool. *Eur J Med Res*. 2023;28:312.
- Wei X, Yang X, Han ZP, Qu FF, Shao L, Shi YF. Mesenchymal stem cells: a new trend for cell therapy. *Acta Pharmacol Sin*. 2013;34:747–54.
- Xing L, Song E, Yu CY, Jia XB, Ma J, Sui MS, et al. Bone marrow-derived mesenchymal stem cells attenuate tubulointerstitial injury through multiple mechanisms in UUO model. *J Cell Biochem*. 2019;120:9737–46.
- Fang TC, Pang CY, Chiu SC, Ding DC, Tsai RK. Renoprotective effect of human umbilical cord-derived mesenchymal stem cells in immunodeficient mice suffering from acute kidney injury. *PLoS ONE*. 2012;7: e46504.
- Chen Y, Qian H, Zhu W, Zhang X, Yan Y, Ye S, et al. Hepatocyte growth factor modification promotes the amelioration effects of human umbilical cord mesenchymal stem cells on rat acute kidney injury. *Stem Cells Dev*. 2011;20:103–13.
- Huang J, Cao H, Cui B, Ma X, Gao L, Yu C, et al. Mesenchymal stem cells-derived exosomes ameliorate ischemia/reperfusion induced acute kidney injury in a porcine model. *Front Cell Dev Biol*. 2022;10: 899869.
- Shi W, Zhou X, Li X, Peng X, Chen G, Li Y, et al. Human umbilical cord mesenchymal stem cells protect against renal ischemia-reperfusion injury by secreting extracellular vesicles loaded with miR-148b-3p that target pyruvate dehydrogenase kinase 4 to inhibit endoplasmic reticulum stress at the reperfusion stages. *Int J Mol Sci*. 2023;24:8899.
- Wang Y, Liu J, Wang H, Lv S, Liu Q, Li S, et al. Mesenchymal stem cell-derived exosomes ameliorate diabetic kidney disease through the NLRP3 signaling pathway. *Stem Cells*. 2023;41:368–83.
- Soekmadji C, Li B, Huang Y, Wang H, An T, Liu C, et al. The future of extracellular vesicles as theranostics—an ISEV meeting report. *J Extracell Vesicles*. 2020;9:1809766.
- Murphy MB, Moncivais K, Caplan AI. Mesenchymal stem cells: environmentally responsive therapeutics for regenerative medicine. *Exp Mol Med*. 2013;45: e54.
- Wang R, Lin M, Li L, Li L, Qi G, Rong R, et al. Bone marrow mesenchymal stem cell-derived exosome protects kidney against ischemia reperfusion injury in rats. *Zhonghua Yi Xue Za Zhi*. 2014;94:3298–303.
- Zou X, Gu D, Zhang G, Zhong L, Cheng Z, Liu G, et al. NK cell regulatory property is involved in the protective role of MSC-derived extracellular vesicles in renal ischemic reperfusion injury. *Hum Gene Ther*. 2016;27:926–35.
- Zou X, Zhang G, Cheng Z, Yin D, Du T, Ju G, et al. Microvesicles derived from human Wharton's Jelly mesenchymal stromal cells ameliorate renal ischemia-reperfusion injury in rats by suppressing CX3CL1. *Stem Cell Res Ther*. 2014;5:40.
- Zou X, Lin S, Zhong L, Liu J, Meng Y, Zhu Y, et al. Renal denervation alleviates renal ischemic reperfusion injury-induced acute and chronic kidney injury in rats partly by modulating miRNAs. *Clin Exp Nephrol*. 2022;26:13–21.
- Parmar K, Mauch P, Vergilio JA, Sackstein R, Down JD. Distribution of hematopoietic stem cells in the bone marrow according to regional hypoxia. *Proc Natl Acad Sci U S A*. 2007;104:5431–6.
- Basciano L, Nemos C, Foliguet B, de Isla N, de Carvalho M, Tran N, et al. Long term culture of mesenchymal stem cells in hypoxia promotes a genetic program maintaining their undifferentiated and multipotent status. *BMC Cell Biol*. 2011;12:12.
- Ejtehadifar M, Shamsasenjan K, Movassaghpour A, Akbarzadehaleh P, Dehdilani N, Abbasi P, et al. The effect of hypoxia on mesenchymal stem cell biology. *Adv Pharm Bull*. 2015;5:141–9.
- Li W, Chen X, Zou F, He X. Extracellular vesicles derived from hypoxia-treated human adipose stem cells increase proliferation and angiogenic differentiation in human adipose stem cells. *Aesthet Surg J*. 2023;43:924–33.
- Majmundar AJ, Wong WJ, Simon MC. Hypoxia-inducible factors and the response to hypoxic stress. *Mol Cell*. 2010;40:294–309.
- Song S, Zhang G, Chen X, Zheng J, Liu X, Wang Y, et al. HIF-1 α increases the osteogenic capacity of ADSCs by coupling angiogenesis and osteogenesis via the HIF-1 α /VEGF/AKT/mTOR signaling pathway. *J Nanobiotechnology*. 2023;21:257.
- Lee JH, Yoon YM, Lee SH. Hypoxic preconditioning promotes the bioactivities of mesenchymal stem cells via the HIF-1 α -GRP78-Akt axis. *Int J Mol Sci*. 2017;18:1320.
- Feng XD, Zhou JH, Chen JY, Feng B, Hu RT, Wu J, et al. Long non-coding RNA SNHG16 promotes human placenta-derived mesenchymal stem cell proliferation capacity through the PI3K/AKT pathway under hypoxia. *World J Stem Cells*. 2022;14:714–28.
- Pincela Lins PM, Pirllet E, Szymonik M, Bronckaers A, Nelissen I. Manufacture of extracellular vesicles derived from mesenchymal stromal cells. *Trends Biotechnol*. 2023;41:965–81.
- Lamichhane TN, Sokic S, Schardt JS, Raiker RS, Lin JW, Jay SM. Emerging roles for extracellular vesicles in tissue engineering and regenerative medicine. *Tissue Eng Part B Rev*. 2015;21:45–54.
- Kwon S, Shin S, Do M, Oh BH, Song Y, Bui VD, et al. Engineering approaches for effective therapeutic applications based on extracellular vesicles. *J Control Release*. 2021;330:15–30.
- Collino F, Lopes JA, Correa S, Abdelhay E, Takiya CM, Wendt CHC, et al. Adipose-derived mesenchymal stromal cells under hypoxia: changes in extracellular vesicles secretion and improvement of renal recovery after ischemic injury. *Cellular Physiol Biochem: Int J Exp Cellular Physiol, Biochem Pharmacol*. 2019;52:1463–83.
- Mao CY, Zhang TT, Li DJ, Zhou E, Fan YQ, He Q, et al. Extracellular vesicles from hypoxia-preconditioned mesenchymal stem cells alleviates myocardial injury by targeting thioredoxin-interacting protein-mediated hypoxia-inducible factor-1 α pathway. *World J Stem Cells*. 2022;14:183–99.

31. Guo J, Jayaprakash P, Dan J, Wise P, Jang GB, Liang C, et al. PRAS40 connects microenvironmental stress signaling to exosome-mediated secretion. *Mol Cell Biol*. 2017. <https://doi.org/10.1128/MCB.00171-17>.
32. Gao X, Yang H, Su J, Xiao W, Ni W, Gu Y. Aescin Protects Neuron from Ischemia-Reperfusion Injury via Regulating the PRAS40/mTOR Signaling Pathway. *Oxid Med Cell Longev*. 2020;2020:7815325.
33. Gregorius J, Wang C, Stambouli O, Hussner T, Qi Y, Tertel T, et al. Small extracellular vesicles obtained from hypoxic mesenchymal stromal cells have unique characteristics that promote cerebral angiogenesis, brain remodeling and neurological recovery after focal cerebral ischemia in mice. *Basic Res Cardiol*. 2021;116:40.
34. Peng X, Liang B, Wang H, Hou J, Yuan Q. Hypoxia pretreatment improves the therapeutic potential of bone marrow mesenchymal stem cells in hindlimb ischemia via upregulation of NRG-1. *Cell Tissue Res*. 2022;388:105–16.
35. Peng X, Liu J, Ren L, Liang B, Wang H, Hou J, et al. Extracellular vesicles derived from hypoxia-preconditioned bone marrow mesenchymal stem cells ameliorate lower limb ischemia by delivering miR-34c. *Mol Cell Biochem*. 2023;478:1645–58.
36. Zhang W, Liu L, Huo Y, Yang Y, Wang Y. Hypoxia-pretreated human MSCs attenuate acute kidney injury through enhanced angiogenic and antioxidative capacities. *Biomed Res Int*. 2014;2014: 462472.
37. Qiu G, Zheng G, Ge M, Wang J, Huang R, Shu Q, et al. Functional proteins of mesenchymal stem cell-derived extracellular vesicles. *Stem Cell Res Ther*. 2019;10:359.
38. Meldolesi J. Unconventional protein secretion dependent on two extracellular vesicles: exosomes and ectosomes. *Front Cell Dev Biol*. 2022;10: 877344.
39. Eirin A, Zhu XY, Puranik AS, Tang H, McGurran KA, van Wijnen AJ, et al. Mesenchymal stem cell-derived extracellular vesicles attenuate kidney inflammation. *Kidney Int*. 2017;92:114–24.
40. Aparicio-Trejo OE, Aranda-Rivera AK, Osorio-Alonso H, Martinez-Klimova E, Sanchez-Lozada LG, Pedraza-Chaverri J, et al. Extracellular vesicles in redox signaling and metabolic regulation in chronic kidney disease. *Antioxidants (Basel)*. 2022;11:356.
41. Cuevas-Lopez B, Romero-Ramirez EI, Garcia-Arroyo FE, Tapia E, Leon-Contreras JC, Silva-Palacios A, et al. NAC pre-administration prevents cardiac mitochondrial bioenergetics, dynamics, biogenesis, and redox alteration in folic acid-AKI-induced cardio-renal syndrome type 3. *Antioxidants (Basel)*. 2023;12:1592.
42. Cimbaljevic S, Suvakov S, Matic M, Pljesa-Ercegovic M, Pekmezovic T, Radic T, et al. Association of GSTO1 and GSTO2 polymorphism with Risk of end-stage renal disease development and patient survival. *J Med Biochem*. 2016;35:302–11.
43. Kolsch H, Linnebank M, Lutjohann D, Jessen F, Wullner U, Harbrecht U, et al. Polymorphisms in glutathione S-transferase omega-1 and AD, vascular dementia, and stroke. *Neurology*. 2004;63:2255–60.

Publisher's Note

Springer Nature remains neutral with regard to jurisdictional claims in published maps and institutional affiliations.